A Numerical Model for the Search of the Optimum Frequency in Electromagnetic Metal Forming

Ruben Otin

International Center for Numerical Methods in Engineering (CIMNE)
Parque Mediterráneo de la Tecnología (PMT)
c/ Esteve Terradas nº5 - Edificio C3
08860 Castelldefels (Barcelona, Spain)

Corresponding author: R. Otin, e-mail: rotin@cimne.upc.edu
tel.: +34 93 413 41 79, fax: +34 93 413 72 42

Abstract

Electromagnetic forming (EMF) is a high velocity forming technique that reshapes electrically conductive materials by abruptly discharging a bank of capacitors through a coil. The oscillation frequency of the discharge is a key parameter in the design of an EMF system. For a given initial stored energy, there exist a frequency that produces the maximum workpiece deformation. Once we know it, we can set the electrical parameters of the EMF system to make the current intensity oscillate with this optimum frequency. This saves energy and money, preventing also the premature wearing of the coil. The objective of the present paper is to find the optimum frequency of an EMF system. Using the results provided by a finite element model in frequency domain, we are able to obtain the current flowing trough the coil, the Lorentz force acting on the workpiece, a function relating the electrical parameters of the EMF system with frequency and the optimum frequency of the discharge. Our approach can be very useful for coil design and for modeling complex

Preprint submitted to International Journal of Solids and Structures 17th December 2012

three-dimensional geometries. To validate the method presented here, we apply it to tube compression and tube expansion processes and compare our results with those provided by other authors.
Keywords: Electromagnetic forming, optimum frequency, numerical analysis, finite element method, tube bulging, tube compression.

---

1. Introduction

Electromagnetic forming (EMF) is a type of high velocity forming that reshapes electrically conductive materials by means of pulsed electromagnetic fields. The EMF process starts when a capacitor bank is abruptly discharged through a coil. The transient electric current flowing through the coil generates a time-varying magnetic field which induces electric currents in any nearby conductive material. These induced currents flow in the opposite direction to the ones in the coil and, therefore, a repulsive force arises. If this force is strong enough then the workpiece can be reshaped with the help of a die.

As it is reviewed in El-Azab et al. (2003); Fenton and Daehn (1998); Mamalis et al. (2006), the EMF technique described above presents several advantages over other forming technologies (e.g., no tool marks on the workpiece surfaces, no need of lubricants, improved formability, less wrinkling, controlled springback, lower energy cost, etc.). But, to design optimum EMF systems and control their performance, we must be able to calculate efficiently the main parameters involved. This is the aim of this work. More specifically, we focus our attention on the search of the optimum discharge current frequency. In Jablonski and Winkler (1978); Zhang et al. (1995); Haiping

and Chunfeng (2009) is shown that, for a given initial energy, there exists a discharge current frequency for which the deformation of the workpiece is maximum. The use of this optimum frequency saves energy and prevents the premature wearing of the coil.

The frequency of the discharge depends on the values of the resistance, inductance and capacitance of the RLC circuit formed by the capacitor bank, coil, workpiece and connectors. For a given set of coil and workpiece, the current frequency can be controlled by varying the electrical parameters of the part of RLC circuit which is external to the system coil-workpiece. In this work, we control the current frequency by changing the capacitance of the capacitor bank, which can be easily done in practice. In this situation, the correspondence between capacitance and frequency is one-to-one, hence, the search for the optimum frequency is equivalent to the search for the optimum capacitance. In real EMF systems, the capacitor bank has only a discrete set of possible capacitances values. Therefore, in practical terms, the real objective is to find out which one of the available capacitances generates the discharge with a frequency nearest to the optimum.

To find the optimum frequency of an EMF system we can compute the deformation of the workpiece for all the available capacitances and select the value which produces the maximum deformation. This is the approach followed in Haiping and Chunfeng (2009); Zhang et al. (1995); Jablonski and Winkler (1978). This approach has the obvious drawback of being computationally expensive when dealing with complex three-dimensional geometries. On the other hand, in the method proposed in this work, we can fully characterized an EMF system (from the electromagnetic point of view) after solving

the time-harmonic Maxwell's equations for a few frequencies.

In Otin et al. (2012) we explained how to obtain the main electromagnetic parameters of an EMF system (i.e., inductance, resistance, current intensity and Lorentz force) from the time-harmonic Maxwell's equations. In the present paper, we show how to use these parameters to estimate the optimum frequency.

2. Optimum frequency search

To find the optimum frequency we need first to compute the Lorentz force acting on the workpiece for every available capacitance. This is done with the method explained in Otin et al. (2012) and summarized below.

In this work, we perform all the electromagnetic simulations neglecting the workpiece deformation. This is done for a clearer exposition of the method and also because the results obtained with an un-deformed workpiece are a good estimation of the parameters involved in an EMF process. These estimations can be very useful for testing modeling conditions on complex three-dimensional geometries with a low computational cost. On the other hand, if higher precision is required, we can consider our results as the first step of a sequential coupling strategy (see Otin et al. (2012)).

2.1. Lorentz force on the workpiece

Our method starts by solving numerically the time-harmonic Maxwell's equations inside a volume containing the coil and the workpiece. For that, we can use any finite element code in frequency domain able to provide us with the electromagnetic fields $\mathbf{E}(\omega)$ and $\mathbf{H}(\omega)$. In this work, we employed the in-house code called ERMES (see Otin (2011)), which implements in C++ the

finite element formulation explained in Otin (2010). The electromagnetic fields $\mathbf{E}(\omega)$ and $\mathbf{H}(\omega)$ obtained at this step will be used to compute the inductance and the resistance of the system coil-workpiece and the Lorentz force acting on the workpiece.

The next step is to obtain the electrical current $I(t)$ flowing through the coil. The capacitor bank and the system coil-workpiece form a RLC circuit through which current flows $I(t)$ given by the expression

$$I(t) = \frac{V}{\omega_0 L} \exp\left(-\gamma\, t\right) \sin\left(\omega_0\, t\right) \tag{1}$$

with

$$\omega_0 = \sqrt{\frac{1}{LC} - \left(\frac{R}{2L}\right)^2} \tag{2}$$

and

$$\gamma = \frac{R}{2L}. \tag{3}$$

The parameter V in (1) is the value of the initial voltage at the terminals the capacitor bank. V is related with the energy of the discharge U by

$$U = \frac{1}{2} C V^2. \tag{4}$$

The inductance L, resistance R and capacitance C of the RLC circuit are defined, respectively, by $L = L_{cb} + L_{con} + L_{cw}$, $R = R_{cb} + R_{con} + R_{cw}$ and $C = C_{cb}$, where the subscript *cb* denotes the parameters of capacitor bank, the subscript *con* denotes the parameters of the connectors between capacitor bank and coil and the subscript *cw* denotes the parameters of system coil-workpiece. The parameters R_{cb}, L_{cb}, R_{con}, L_{con} and C_{cb} are given data, while R_{cw} and L_{cw} are obtained from Jackson (1999)

$$R_{cw}(\omega) = \frac{1}{|I_n|^2} \int_v \sigma |\mathbf{E}(\omega)|^2 \, dv \tag{5}$$

$$L_{cw}(\omega) = \frac{1}{|I_n|^2} \int_{\upsilon} \mu |\mathbf{H}(\omega)|^2 \, d\upsilon, \tag{6}$$

where σ is the electrical conductivity, μ is the magnetic permeability, υ is a volume containing the coil and the workpiece and I_n is the current injected into the system through the input terminals. Inside the volume of the coil we replace equation (5) by

$$R_{cw}(\omega) = \frac{1}{|I_n|^2} \int_{\upsilon} \frac{|\mathbf{J}|^2}{\sigma} \, d\upsilon \tag{7}$$

where $\mathbf{J}$ includes the imposed and induced current densities ($\mathbf{J} = \mathbf{J}_{imp} + \sigma\mathbf{E}$) and σ is the conductivity of the coil.

Reordering equation (2) we deduce the one-to-one relation between frequency and capacitance

$$C(\omega) = \frac{4L(\omega)}{4\omega^2 L(\omega)^2 + R(\omega)^2}. \tag{8}$$

Once C_{cb} is fixed, the frequency of the discharge ω_0 is the solution of the equation $C(\omega) = C_{cb}$. Because we have neglected the workpiece deformation, the frequency ω_0 and the total inductance L and resistance R remain constant during the discharge. On the other hand, if we were to consider the deformation of the workpiece, the resistance R_{cw} and inductance L_{cw} will change as the workpiece deforms and, therefore, ω_0, R and L also will change with time.

Finally, the Lorentz force acting on the workpiece is given by the expression

$$\mathbf{f}(\mathbf{r}, t) = \mathbf{J}(\mathbf{r}, t) \times \mathbf{B}(\mathbf{r}, t) = \sigma\mu \left(\mathbf{E}(\mathbf{r}, t) \times \mathbf{H}(\mathbf{r}, t) \right), \tag{9}$$

where $\mathbf{r}$ is a point inside the workpiece, $\mathbf{J} = \sigma\mathbf{E}$ is the induced current density and $\mathbf{B} = \mu\mathbf{H}$ is the magnetic flux density. The fields $\mathbf{E}(\mathbf{r}, t)$ and $\mathbf{H}(\mathbf{r}, t)$ are

related with $\mathbf{E}(\mathbf{r},\omega)$ and $\mathbf{H}(\mathbf{r},\omega)$ by

$$\mathbf{E}(\mathbf{r},t) = \frac{1}{2\pi}\int_{-\infty}^{\infty} \mathbf{E}_n(\mathbf{r},\omega)\, I(\omega)\, e^{i\omega t}\, d\omega, \tag{10}$$

$$\mathbf{H}(\mathbf{r},t) = \frac{1}{2\pi}\int_{-\infty}^{\infty} \mathbf{H}_n(\mathbf{r},\omega)\, I(\omega)\, e^{i\omega t}\, d\omega, \tag{11}$$

where $i = \sqrt{-1}$ is the imaginary unit, $\mathbf{E}_n(\mathbf{r},\omega)$ and $\mathbf{H}_n(\mathbf{r},\omega)$ are the fields per unit intensity at the frequency ω and $I(\omega)$ is the Fourier transform of the intensity $I(t)$ given in equation (1). The fields per unit intensity are defined by

$$\mathbf{E}_n(\mathbf{r},\omega) = \frac{\mathbf{E}(\mathbf{r},\omega)}{I_n}, \tag{12}$$

$$\mathbf{H}_n(\mathbf{r},\omega) = \frac{\mathbf{H}(\mathbf{r},\omega)}{I_n}, \tag{13}$$

where $\mathbf{E}(\mathbf{r},\omega)$, $\mathbf{H}(\mathbf{r},\omega)$ and I_n are the fields and intensity appearing in equations (5) and (6).

2.2. Optimum frequency and capacitance

To obtain the optimum frequency ω_{op}, we set the initial charging energy at a fixed value U_0 and look for the frequency which produces the maximum momentum $\mathbf{P}$ in the first n semi-periods, where a semi-period is half of a period $T/2 = \pi/\omega$. That is, we look for the frequency which makes maximum the quantity

$$\Delta\mathbf{P}_n = \int_0^{\frac{n\pi}{\omega}} \mathbf{F}_{tot} \cdot dt, \tag{14}$$

where $\mathbf{F}_{tot}$ is the total magnetic force acting on the workpiece and $\Delta\mathbf{P}_n$ is the momentum produced by this force in the first n semi-periods. The number n must be selected with care, if we use a high n then the frequency ω_{op} will

be too high and if n is too low then ω_{op} will be too low. The number of semi-periods we select is the minimum natural number n which accomplish

$$n \geq \frac{2\,L\,\omega_{\infty}}{\pi\,R}, \tag{15}$$

where ω_{∞} is the frequency which makes maximum the quantity $\Delta\mathbf{P}_{\infty}$ and L and R are the inductance and the resistance evaluated at ω_{∞}. The quantity $\Delta\mathbf{P}_{\infty}$ is obtained when $n \to \infty$ in equation (14). Equation (15) comes from reordering $(n\pi/\omega) \geq (1/\gamma)$, where γ is defined in equation (3). The minimum natural number which satisfies the inequality (15) represents the minimum number of semi-periods required to release more than 80% of the total momentum $\Delta\mathbf{P}_{\infty}$.

In summary, we first locate the frequency ω_{∞} which makes maximum the quantity $\Delta\mathbf{P}_{\infty}$. Second, we compute n with equation (15). Finally, ω_{op} is the frequency which makes maximum $\Delta\mathbf{P}_{n}$, being n the natural number calculated in the second step. All this process is performed neglecting the workpiece deformation. We do not require any additional simulation. We are using the data obtained in the initial frequency sweep of our electromagnetic model. It takes only a few seconds to compute all the integrals and obtain ω_{op}.

We perform the integral of equation (14) only along the first n semi-periods because only the first semi-periods have an important contribution in a real EMF process. This is so because the magnetic force acting on the workpiece decreases dramatically when the workpiece starts to deform and moves away from the coil. Thus, if we make $n \to \infty$, we are considering too many pulses without a significant contribution in a real EMF process. But, on the other hand, if we make $n = 1$, we are neglecting pulses that are able to

contribute to the deformation of the workpiece even though they come after the first more energetic pulses. Therefore, the selection of the number n must be a compromise between taking the minimum number of pulses (only the first pulses has a real contribution) and considering all the *enough-energetic* secondary pulses (secondary pulses that can have enough energy to deform the workpiece). These two criteria are fulfilled in the equation (15). The n obtained with equation (15) is the minimum natural number guaranteeing that, on the first n semi-periods, it has been released, at least, 80% of the total momentum that can be released at every frequency.

Because we have neglected the workpiece deformation, the optimum frequency calculated with equation (14) (or, equivalently, the optimum capacitance, after using equation (8)) must be considered as an initial guess. This initial guess reduces the number of necessary tests (electro-mechanical simulations or experimental measurements) which have to be performed to ensure the setting of the EMF system parameters in its optimum values. In fact, if the initial guess is good enough, we can be sure of finding the real optimum value with only three tests. For instance, suppose that our initial guess falls between two available capacitances C_1 and C_2, being $C_1 < C_2$. We make two tests and obtain that the deflections h of the workpiece satisfy $h_1 < h_2$. Afterwards, we take a capacitance C_3 which is the lower value available such as $C_2 < C_3$. If we compute (or measure) that $h_2 > h_3$ then C_2 is the optimum capacitance. In this case, we have required only three tests. On the other hand, if $h_2 < h_3$, we must keep on testing with successive C_n until find a h_n such as $h_n > h_{n+1}$. When this happens, we have that C_n is the optimum capacitance and $n + 1$ the number of tests. Therefore, the better

the initial guess is, the less electro-mechanical simulations, or experimental measurements, must be performed to set an EMF system in its optimum values.

3. Application example I. Tube expansion.

In this section we apply the electromagnetic model explained above to the EMF process showed in Zhang et al. (1995). This process consists in the expansion of a cylindrical tube by a solenoidal coil under different working conditions. In Zhang et al. (1995), the tube bulging process is analyzed for several coils lengths $\ell = \{100,\ 200,\ 300,\ 400,\ 500\}\,\mathrm{mm}$, capacitances $C_{cb} = \{24,\ 50,\ 100,\ 200,\ 400,\ 800,\ 1600\}\,\mu\mathrm{F}$ and initial charging energies $U = \{1,\ 2\}\,\mathrm{kJ}$.

The coil is made of $d = 2.0\,\mathrm{mm}$ diameter copper wire with an electrical conductivity of $\sigma = 58.0 \times 10^6\,\mathrm{S/m}$. The outer diameter of the coil is $D_c = 37.0\,\mathrm{mm}$ and the separation between each loop is $p = 3.0\,\mathrm{mm}$. The coil is approximated by coaxial loop currents, concentric with the workpiece and placed inside it. Thus, the problem is considered axis symmetric.

The workpiece is a cylindrical tube made of annealed aluminum A1050TD of outer diameter $D_{wp} = 40.0\,\mathrm{mm}$, thickness $\tau = 1.0\,\mathrm{mm}$ and electrical conductivity $\sigma = 36.0 \times 10^6\,\mathrm{S/m}$. We assume that $\epsilon = \epsilon_0$ and $\mu = \mu_0$ for workpiece and coil.

In Zhang et al. (1995) is said that L_{cb} and R_{cb} are less than $1.0\,\mu\mathrm{H}$ and $2.0\,\mathrm{m}\Omega$ respectively. But, in Motoasca (2003), where it is used an EMF set-up similar to that used in Zhang et al. (1995), it is reached to the conclusion that these quantities do not take into account the inductance L_{con} and the

resistance R_{con} of the wires connecting the capacitor bank with the coil. In Motoasca (2003) is found that $L_{cb} + L_{con} = 2.5\,\mu\text{H}$ and $R_{cb} + R_{con} = 15.0\,\text{m}\Omega$ are more realistic values for the electrical parameters external to the system coil-workpiece. Then, in this work, we consider $R(\omega) = R_{cw}(\omega) + 15.0\,\text{m}\Omega$ and $L(\omega) = L_{cw}(\omega) + 2.5\,\mu\text{H}$ as the total resistance and inductance of the RLC circuit formed by the capacitor bank and the system coil-workpiece.

3.1. Lorentz force on the workpiece

As remarked at the beginning of section 2, we need to compute the Lorentz force acting on the workpiece before obtaining the optimum frequency. In this subsection we are going to illustrate the method summarized in 2.1. We want to mention before start the description that, in the current stage of development, we put more emphasis in the accuracy of the solutions than in the computational performance of the method. That is, we employed fine FEM meshes and small frequency steps to guarantee accurate solutions despite the increase in the computational cost. As it will become evident later in this section, we can reduce the number of simulations and calculate each frequency in parallel and independently of one another to improve globally the computational performance of the method.

First of all, we compute the fields $\mathbf{E}(\mathbf{r}, \omega)$ and $\mathbf{H}(\mathbf{r}, \omega)$ with the finite element tool ERMES. We calculate the fields for the frequencies in the interval $f \in [0, 40]\,\text{kHz}$ with a frequency step of $\Delta f = 1\,\text{Hz}$ (see Otin et al. (2012) for details about the selection of the frequency interval). It is only necessary to compute the fields for positive frequencies because $\mathbf{E}_n(\omega) = \mathbf{E}_n(-\omega)$ and $\mathbf{H}_n(\omega) = \mathbf{H}_n(-\omega)$. The time required to calculate the fields for each frequency was less than 30 seconds in a desktop computer with a CPU Intel

Core 2 Quad Q9300 at 2.5 GHz, 8 GB of RAM memory and the operative system Microsoft Windows XP Professional x64 Edition v2003. In figures 1 and 2 we show the modulus of the normalized fields $\mathbf{E}_n(\mathbf{r},\omega)$ and $\mathbf{H}_n(\mathbf{r},\omega)$, respectively, at the frequency $f = \omega/2\pi = 4.6\,\mathrm{kHz}$. In figure 3 we can appreciate the electrical current density in the coil and workpiece and how the current density distribution inside the coil is affected by the proximity of the workpiece.

In figure 4 we graph the evolution of $|\mathbf{H}_n(\omega)|$ with the frequency. This graph shows the slow variation of the fields with frequency. As a consequence of this slow variation, we can increase the frequency step Δf and reduce the total number of simulations. If we need to know the fields at frequencies which has not been simulated we can obtain these fields by a linear combination of the fields yet calculated. Therefore, we can characterize electromagnetically an EMF system after solving the time-harmonic Maxwell's equations for only a few frequencies.

Once the fields are known, we can use equations (5) and (6) to calculate the resistance and the inductance of the RLC circuit formed by the coil, workpiece and capacitor bank. The resistance and inductance for the case of coil length $\ell = 200\,\mathrm{mm}$ ($N = 68$ turns), is plotted in figures 5 and 6 respectively. In figure 7, equation (8) is plotted for the same case $\ell = 200\,\mathrm{mm}$. In figure 8 we show the calculated intensity for the capacitances $C_{cb} = \{160,\, 800\}\,\mu\mathrm{F}$ and initial charging energy $U = 2\,\mathrm{kJ}$. For the case of $C_{cb} = 160\,\mu\mathrm{F}$ we found that $f_0 = \omega_0/2\pi = 4.6\,\mathrm{kHz}$, $L(\omega_0) = 6.9\,\mu\mathrm{H}$ and $R(\omega_0) = 110.1\,\mathrm{m}\Omega$. For the case of $C_{cb} = 800\,\mu\mathrm{F}$ we found that $f_0 = 1.7\,\mathrm{kHz}$, $L(\omega_0) = 8.3\,\mu\mathrm{H}$ and $R(\omega_0) = 102.8\,\mathrm{m}\Omega$. To obtain these values we only need to find f_0 in the

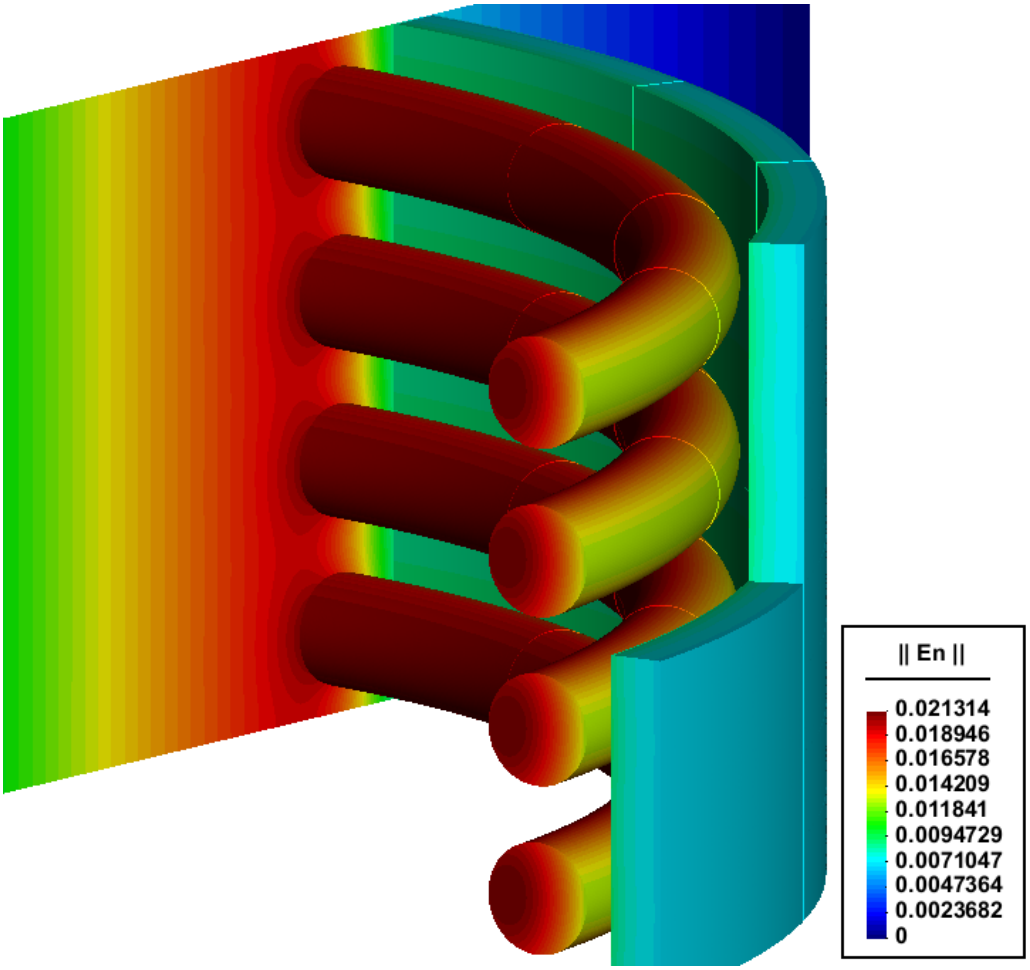

Figure 1: Modulus of the normalized electric field $\mathbf{E}_n(\mathbf{r}, \omega)$ at $f = 4.6\,\text{kHz}$ in the cental part of the system coil-workpiece described in section 3.

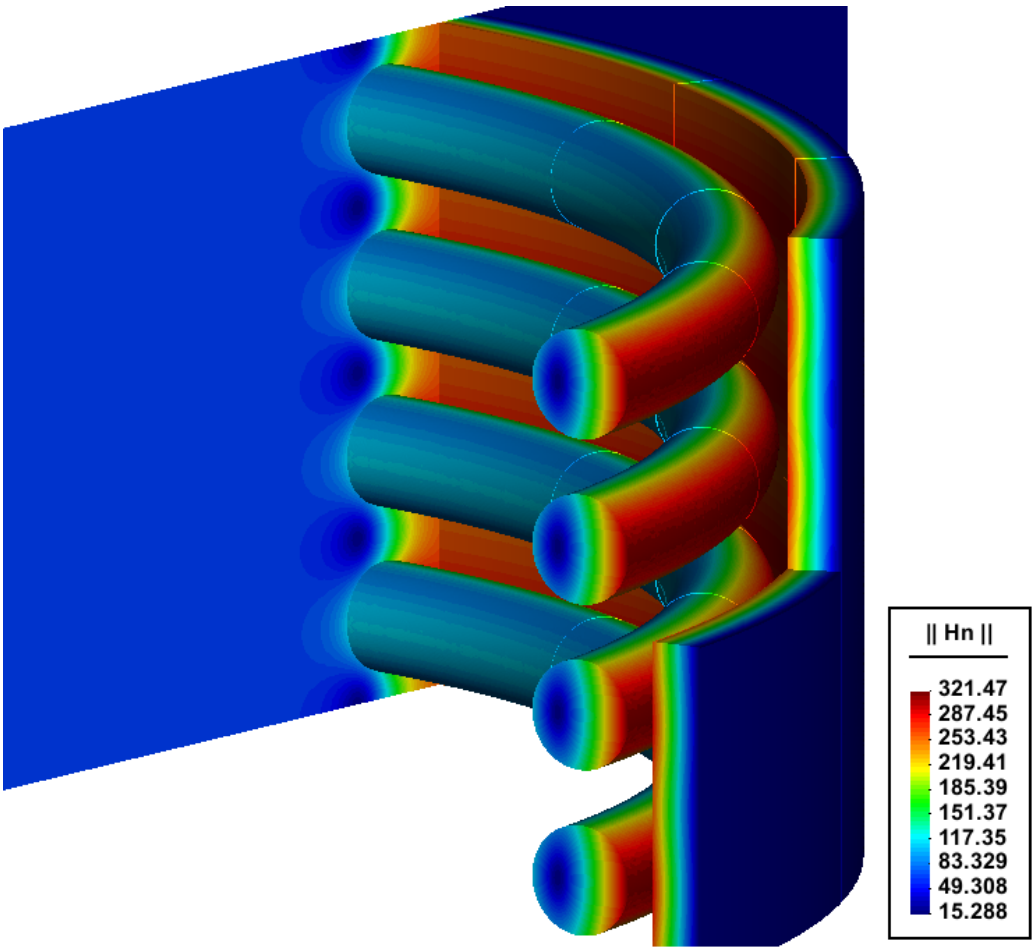

Figure 2: Modulus of the normalized magnetic field $\mathbf{H}_n(\mathbf{r}, \omega)$ at $f = 4.6\,\text{kHz}$ in the cental part of the system coil-workpiece described in section 3.

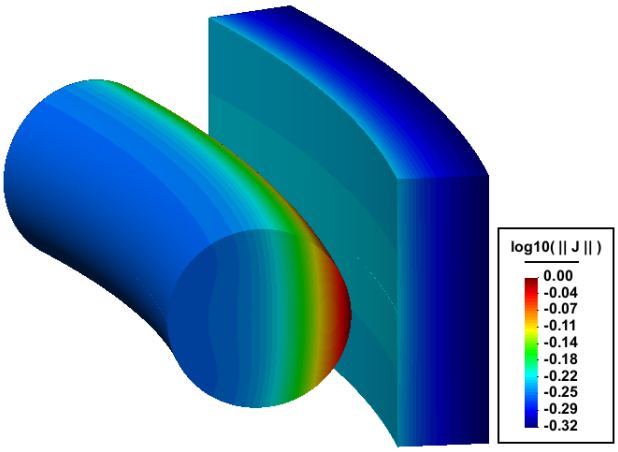

Figure 3: Modulus of the current density $\mathbf{J}$ in logarithm scale at $f = 4.6\,\mathrm{kHz}$. The current density has been normalized to its maximum value. The proximity effect is clearly appreciated.

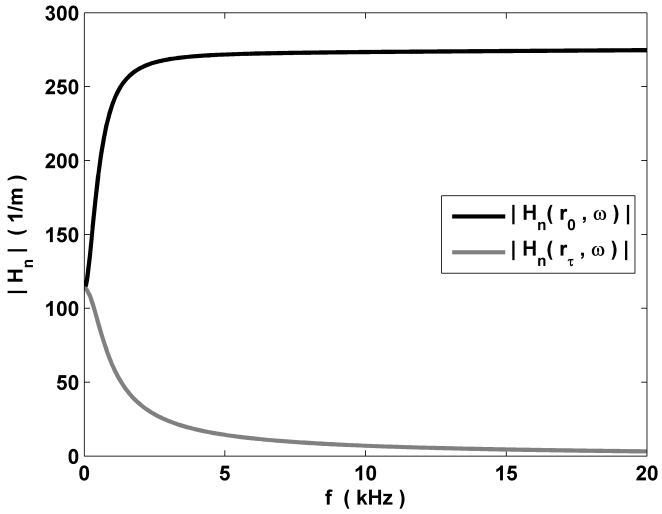

Figure 4: Modulus of the normalized magnetic field $\mathbf{H}_n(\omega)$ as a function of the frequency $f = \omega/2\pi$ on a point $\mathbf{r}_0$ located at the inner surface of the tube and on a point $\mathbf{r}_\tau$ located on the outer surface of the tube.

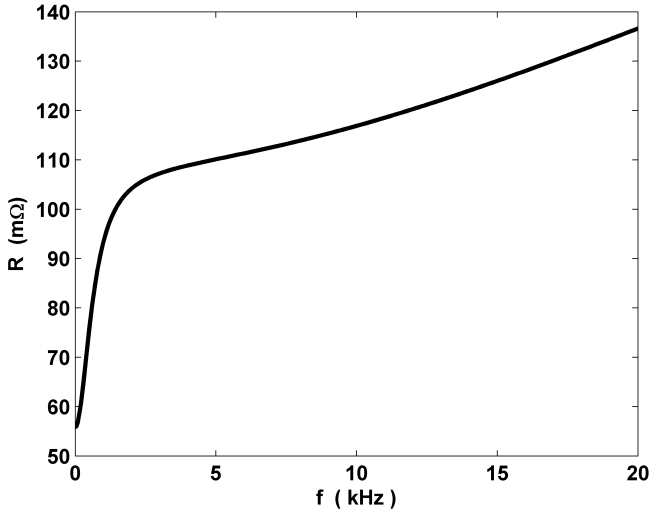

Figure 5: Total resistance R of the RLC circuit formed by the capacitor bank and the system coil-workpiece (coil length $\ell = 200\,\mathrm{mm}$) as a function of the frequency f.

graph of figure 7 and substitute this frequency in the functions $L(\omega)$ and $R(\omega)$. Following this method, we calculated the maximum current intensity for several coil lengths ℓ and capacitances C_{cb} (see figure 9).

Once the capacitance C_{cb} is fixed and the intensity known, we can calculate the Fourier transform of $I(t)$. The Fourier transform of the intensity given by equation (1) has the following analytical expression

$$I(\omega) = \frac{1}{2}\left(\frac{1}{\omega + \omega_0 - i\gamma_0} - \frac{1}{\omega - \omega_0 - i\gamma_0}\right), \tag{16}$$

where ω_0 is the frequency (2) and γ_0 is the parameter (3). In figure 10 is represented equation 16 for the cases $C_{cb} = 160\,\mu\mathrm{F}$ and $C_{cb} = 800\,\mu\mathrm{F}$. With equation (16), the fields computed with ERMES, and equations (10) and (11) we obtain $\mathbf{E}(\mathbf{r}, t)$ and $\mathbf{H}(\mathbf{r}, t)$ at any point $\mathbf{r}$ of the problem domain and at any time t.

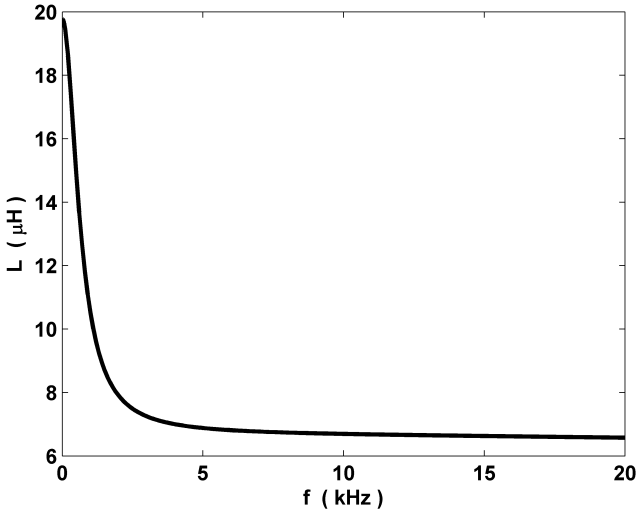

Figure 6: Total inductance L of the RLC circuit formed by the capacitor bank and the system coil-workpiece (coil length $\ell = 200\,\mathrm{mm}$) as a function of the frequency f.

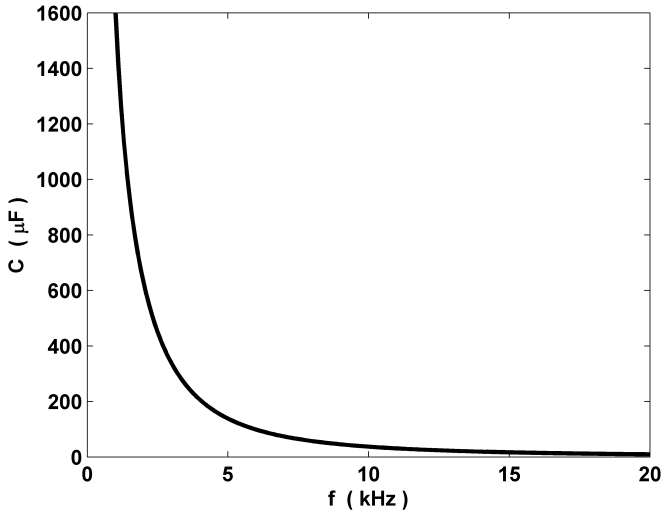

Figure 7: Capacitance C of the RLC circuit with coil length $\ell = 200\,\mathrm{mm}$ as a function of the frequency f.

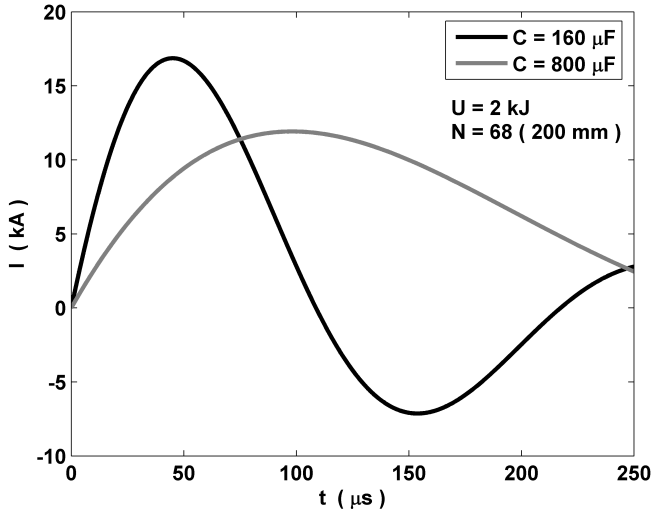

Figure 8: Intensity flowing trough the coil of length $\ell = 200\,\mathrm{mm}$ ($N = 68$ turns) for the capacitances $C_{cb} = \{160,\ 800\}\,\mu\mathrm{F}$ and initial charging energy $U = 2\,\mathrm{kJ}$.

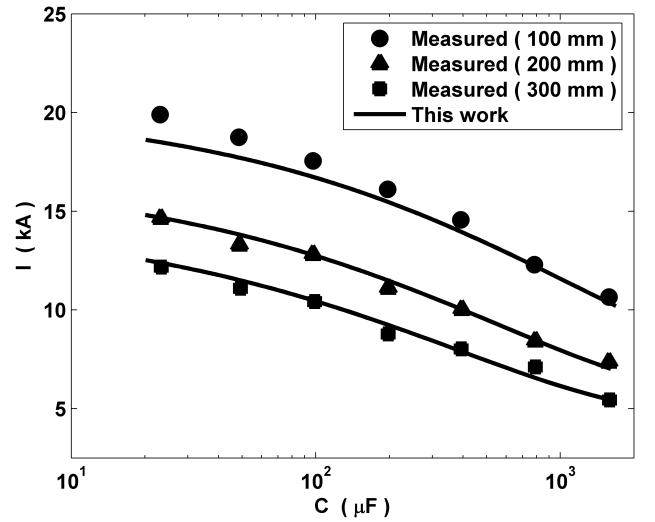

Figure 9: Maximum current intensity for several coil lengths ℓ and capacitances C_{cb}. The initial charging energy is $U = 1\,\mathrm{kJ}$ in all the cases. Measurements from Zhang et al. (1995).

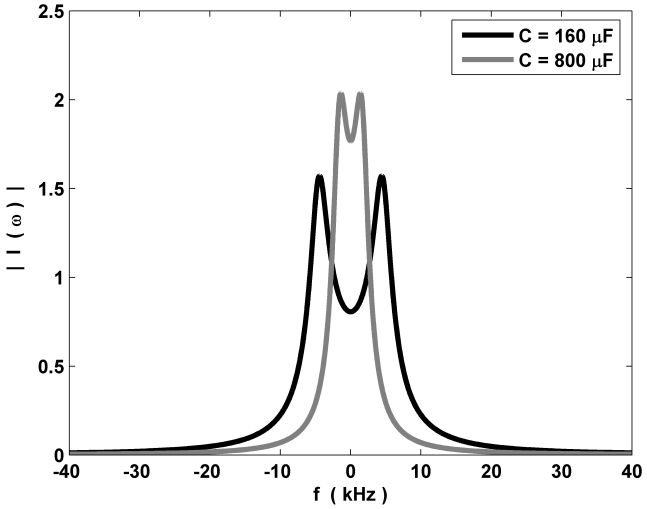

Figure 10: Modulus of the Fourier transform of the intensities showed in figure 8 ($\ell = 200\,\mathrm{mm}$, $C_{cb} = \{160,\ 800\}\,\mu\mathrm{F}$ and $U = 2\,\mathrm{kJ}$).

The integrals of equations (10) and (11) were evaluated using the trapezoidal rule implemented inside MATLAB (function *trapz*). The functions were integrated in the interval $f \in [-40, 40]\,\mathrm{kHz}$ with a step of $\Delta f = 1\,\mathrm{Hz}$. The main contribution to the integrals of equations (10) and (11) comes from the frequencies in the close vicinity of ω_0. This is due to the peak shape of the function $I(\omega)$ around ω_0 (see figure 10) and the slow variation of the fields with frequency.

We calculated the magnetic pressure over the surfaces of the workpiece (instead of the volumetric Lorentz force given in equation (9)) in order to compare our results with those provided by Zhang et al. (1995). The magnetic pressure used in Zhang et al. (1995) can be written as

$$P(\mathbf{r}_0, t) = \frac{1}{2}\,\mu\left(|\mathbf{H}(\mathbf{r}_0, t)|^2 - |\mathbf{H}(\mathbf{r}_\tau, t)|^2\right), \tag{17}$$

where $\mathbf{r}_0$ is a point placed on the inner surface of the workpiece and $\mathbf{r}_\tau$ is a point placed outside, on the opposite side. Also, we had to average the fields $\mathbf{H}(\mathbf{r}_0, t)$ and $\mathbf{H}(\mathbf{r}_\tau, t)$ over the workpiece surfaces because the simplified model of the coil used in Zhang et al. (1995) produces constant fields over these surfaces. The results for $\ell = 200\,\text{mm}$, $C_{cb} = \{160,\, 800\}\,\mu\text{F}$ and $U = 2\,\text{kJ}$ are shown in figures 11 and 12.

The differences in the results can be attributed to the different features of each model. We used a more realistic electromagnetic model for the coil than Zhang et al. (1995). We take into account effects such as the skin and proximity effects (see figure 3). These effects increment the value of the fields at the coil-workpiece interspace and they are more evident at higher frequencies. These physical phenomena also affects the electrical parameters of the RLC circuit, increasing the value of R_{cw} and decreasing the value of L_{cw} with frequency. Moreover, Zhang et al. (1995) uses an exponential decay approximation of the fields inside the workpiece which is only strictly true for semi-infinite conductive planes. This approximation gives lower values of the magnetic pressure than the ones obtained considering a finite thickness workpiece (as we do). The combined contribution of these effects explains, in part, the differences in the magnetic pressures showed in figures 11 and 12. Also, it explains why the differences are greater in figure 11 ($f_0 = 4.6\,\text{kHz}$) than in figure 12 ($f_0 = 1.7\,\text{kHz}$).

Another source of divergence is that Zhang et al. (1995) considers the movement of the workpiece and, on the other hand, we neglect it. Therefore, the frequency and modulus of the magnetic pressure calculated by Zhang et al. (1995) for the case $C_{cb} = 800\,\mu\text{F}$ (see figure 12) must be closer to

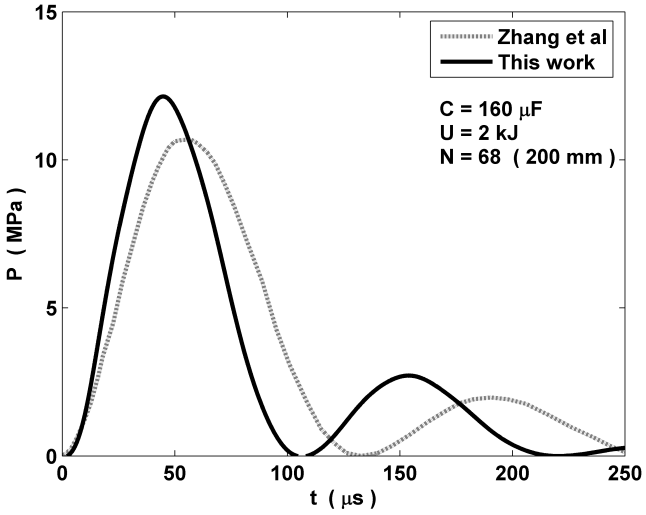

Figure 11: Magnetic pressure on the workpiece for the case of coil length $\ell = 200\,\text{mm}$, $C_{cb} = 160\,\mu\text{F}$ and initial charging energy $U = 2\,\text{kJ}$.

the calculated with our model than in the case $C_{cb} = 160\,\mu\text{F}$ (see figure 11) because the expansion produced in the tube with the capacitance $C_{cb} = 160\,\mu\text{F}$ is larger than the expansion produced using a capacitance of $C_{cb} = 800\,\mu\text{F}$.

3.2. Optimum frequency and capacitance

In Zhang et al. (1995) is computed the bulge height produced by coils of different lengths $\ell = \{100,\ 200,\ 300,\ 400,\ 500\}\,\text{mm}$ and with C_{cb} varying from $20\,\mu\text{F}$ to $1600\,\mu\text{F}$. The optimum capacitance for each coil is the C_{cb} which causes the maximum deformation. The results of Zhang et al. (1995) are summarized in table 1.

We analyzed this problem with the method detailed in section 2.2, that is, we obtained the value of the optimum capacitance C_{op} from the capacitance

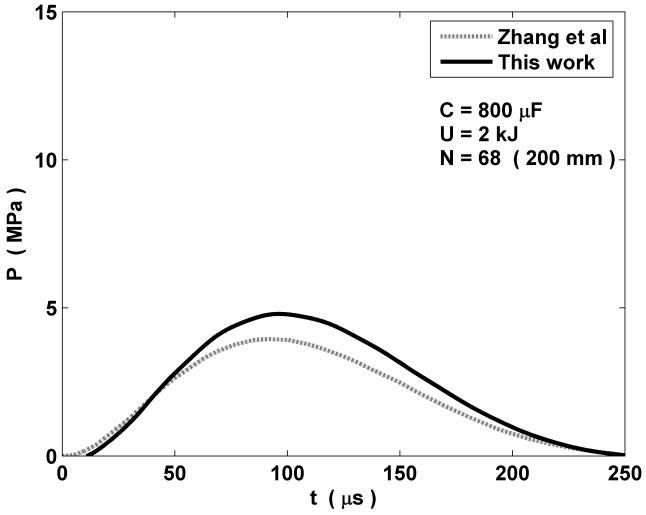

Figure 12: Magnetic pressure on the workpiece for the case of coil length $\ell = 200\,\text{mm}$, $C_{cb} = 800\,\mu\text{F}$ and initial charging energy $U = 2\,\text{kJ}$.

which makes maximum the quantity $\Delta\mathbf{P}_n$ defined in equation (14). The total force was obtained after integrating equation (17) over the workpiece surfaces. The integral of equation (14) was evaluated using the function *trapz* implemented inside MATLAB. The number of semi-periods calculated with equation (15) was $n = 2$ for all the coil lengths. The momentum $\Delta\mathbf{P}_2$ is graphed in figure 13 as a function of the capacitance C_{cb} for the coil lengths $\ell = \{200,\, 300,\, 400,\, 500\}\,\text{mm}$ and the initial charging energy $U = 2\,\text{kJ}$. The values of C_{op} obtained in this work are presented in table 1.

In table 1 we can see that there exists a good correlation between the results provided by Zhang et al. (1995) and our approach. The differences observed at longer coils are due to the modelling differences explained at the end of section 3.1. The values of the optimal capacitance are lower for longer

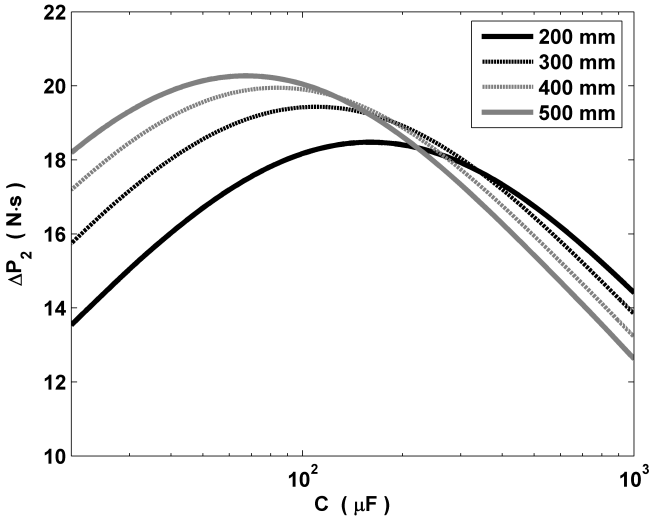

Figure 13: Momentum $\Delta\mathbf{P}_2$ as a function of the capacitance C for the coil lengths $\ell = \{200, 300, 400, 500\}$ mm. The initial charging energy is $U = 2\,\mathrm{kJ}$ in all the cases. The optimum capacitance C_{op} is the one which makes maximum the quantity $\Delta\mathbf{P}_2$. The values of C_{op} are shown in table 1.

coils but, as can be deduced from equation (8), the values of the optimal frequency are higher. As it is explained in section 3.1, it is precisely at higher frequencies when the differences between models are greater.

4. Application example II. Tube compression.

Haiping and Chunfeng (2009) analyzed the compression of a tube by a solenoidal coil for the capacitances $C_{cb} = \{60, 120, 240, 360, 480, 600, 702, 720, 840, 960, 1080, 1800\}\,\mu$F and initial charging energy $U = 2.02\,\mathrm{kJ}$.

The workpiece is made of aluminium AA3003 with an electrical conductivity $\sigma = 29.4 \times 10^6\,\mathrm{S/m}$. The outer diameter of the workpiece is $D_{wp} = 50.0\,\mathrm{mm}$, its thickness is $\tau = 2\,\mathrm{mm}$ and its length is $\ell = 100.0\,\mathrm{mm}$.

ℓ (mm)	C_{op} (μF) Zhang et al.	C_{op} (μF) This work
100	310	296
200	160	161
300	100	108
400	70	83
500	40	67

Table 1: Values of the optimum capacitance (C_{op}) for different coil lengths (ℓ). The C_{op} calculated in Zhang et al. (1995) is compared with the C_{op} calculated in this work.

The solenoidal coil is approximated by coaxial loop currents, concentric with the workpiece and placed outside it. The coil is made of copper with a conductivity $\sigma = 58.0 \times 10^6\,\mathrm{S/m}$. The inner diameter of the coil is $D_c = 56.0\,\mathrm{mm}$. The separation between each loop is $p = 6.25\,\mathrm{mm}$. The length of the coil is $\ell = 100\,\mathrm{mm}$ and the number of turns is $N = 17$. The dimensions of the coil wires are not provided in Haiping and Chunfeng (2009). We assumed a thickness of $\triangle x_c = 5\,\mathrm{mm}$ and a height of $\triangle y_c = 3\,\mathrm{mm}$ for each coil wire.

Haiping and Chunfeng (2009) assumed that $R = R_{cb} + R_{con} + R_{cw} = 13.03\,\mathrm{m\Omega}$ and $L = L_{cb} + L_{con} + L_{cw} = 1.22\,\mu\mathrm{H}$ for all the frequencies. We showed in section 3 that, actually, R and L depend on frequency but, for comparison purposes, we assume that $R = 13.03\,\mathrm{m\Omega}$ and $L = 1.22\,\mu\mathrm{H}$ for all the frequencies.

Haiping and Chunfeng (2009) computed the radial displacement of the walls of the tube for the capacitances C_{cb} listed at the beginning of this section. The maximum displacement took place at $C_{cb} = 840\,\mu\text{F}$ ($f = 4.97\,\text{kHz}$).

In this work, we apply the method of section 2. We start by computing with ERMES the fields $\mathbf{E}(\mathbf{r}, \omega)$ and $\mathbf{H}(\mathbf{r}, \omega)$ (see figures 14 and 15). Then, after obtaining the Lorentz force, we look for the frequency ω_∞ which makes maximum the quantity $\Delta\mathbf{P}_\infty$. This frequency is $f_\infty = \omega_\infty/2\pi = 13\,\text{kHz}$. If we substitute f_∞, R and L in equation (15), we have that $n = 5$. Then, C_{op} is the capacitance which makes maximum the quantity $\Delta\mathbf{P}_5$. In figure 16 we show the momentum $\Delta\mathbf{P}_5$ as a function of the capacitance C_{cb}. The maximum $\Delta\mathbf{P}_5$ is reached at $C_{op} = 805\,\mu\text{F}$ ($f_{op} = 5\,\text{kHz}$). This result is very close to the one obtained by Haiping and Chunfeng (2009) (see table 2). Moreover, we must take into account that Haiping and Chunfeng (2009) only computes the workpiece deformation for a discrete set of capacitances. Then, the optimum capacitance of the set-up showed in Haiping and Chunfeng (2009) could be any value around $840\,\mu\text{F}$ ($4.97\,\text{kHz}$) that were within the range $[720, 960]\,\mu\text{F}$ ($[4.65, 5.37]\,\text{Hz}$).

5. Conclusion

In this paper we have shown a method that numerically solves the time-harmonic Maxwell's equations in a volume containing the coil and the workpiece. Through this method we deduced the current flowing trough the coil, the Lorentz force acting on the workpiece and the optimum frequency of an EMF process. We can obtain the magnitude of the main parameters involved in the design of EMF systems and test modelling conditions on

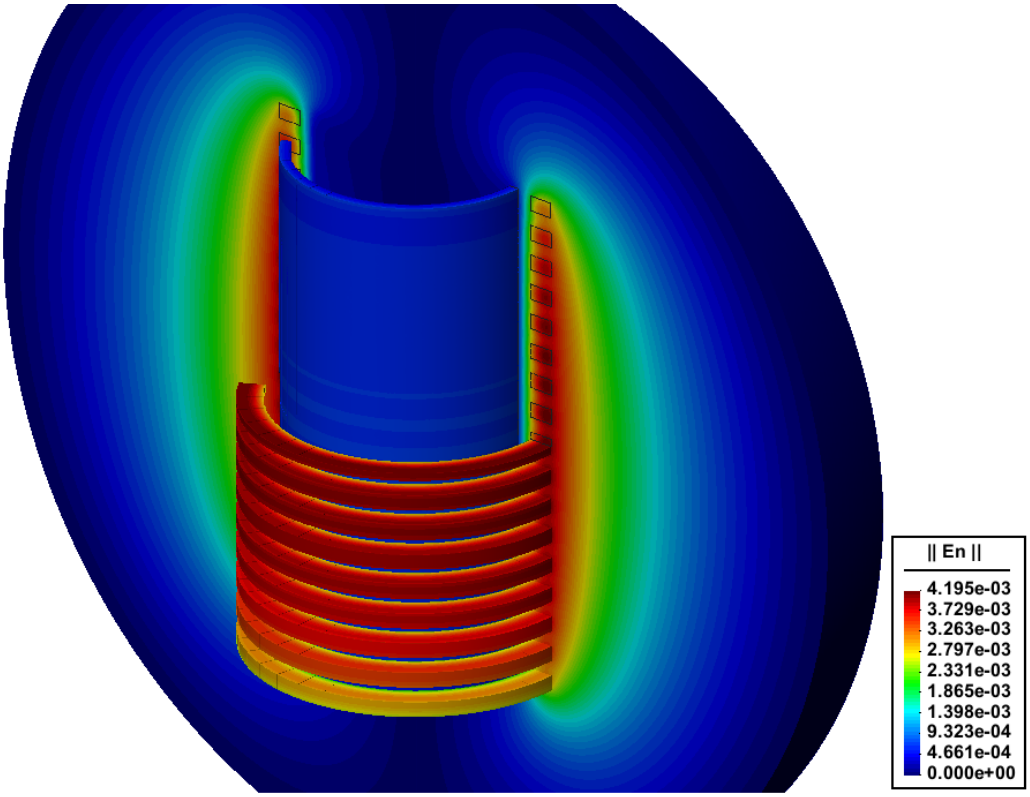

Figure 14: Modulus of the normalized electric field $\mathbf{E}_n(\mathbf{r}, \omega)$ at $f = 5\,\text{kHz}$ for the tube compression process described in section 4.

$C_{op}\,(\mu\text{F})$ Haiping and Chunfeng	$C_{op}\,(\mu\text{F})$ This work
840	805

Table 2: C_{op} calculated in Haiping and Chunfeng (2009) compared with the C_{op} calculated in this work.

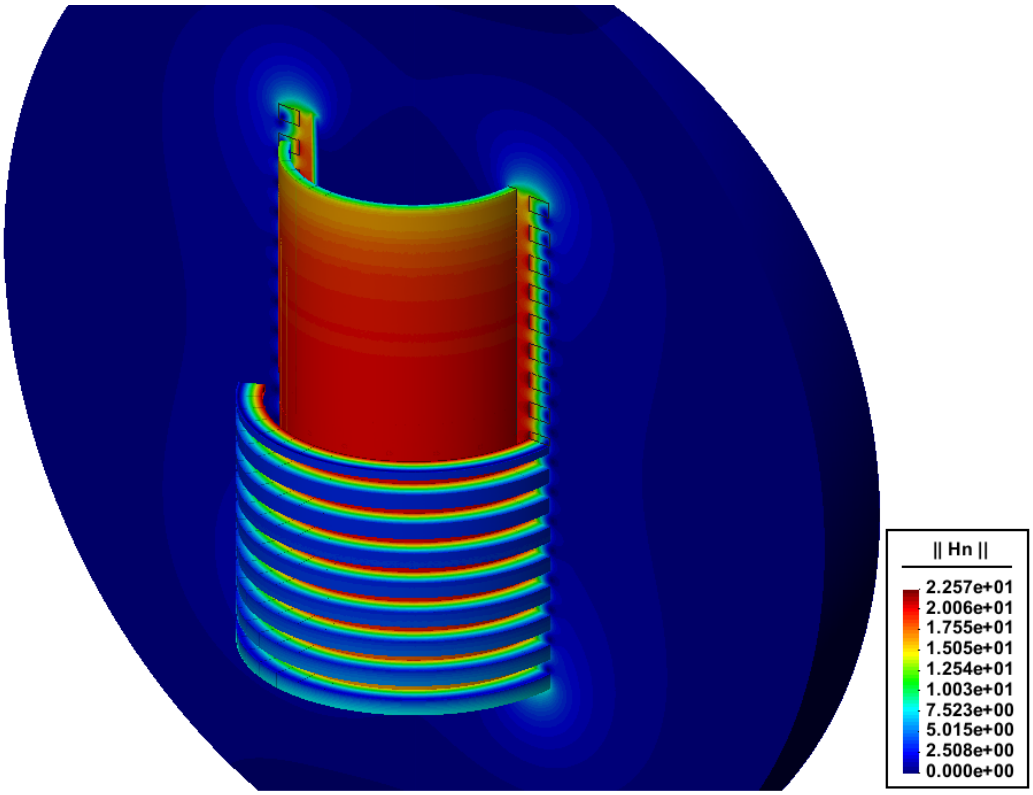

Figure 15: Modulus of the normalized magnetic field $\mathbf{H}_n(\mathbf{r}, \omega)$ at $f = 5\,\text{kHz}$ for the tube compression process described in section 4.

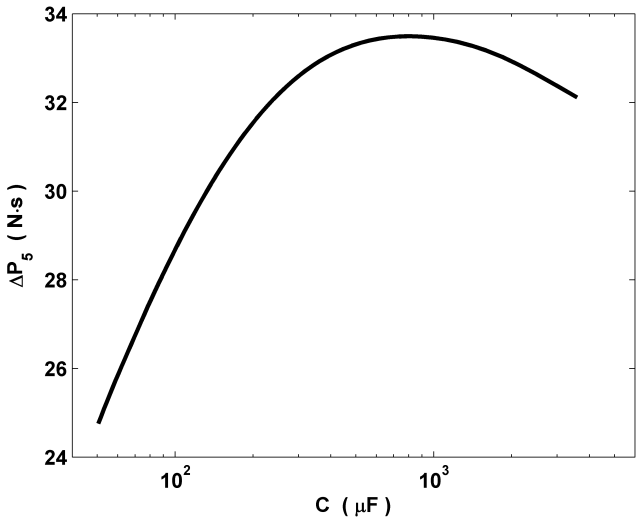

Figure 16: Momentum $\Delta\mathbf{P}_5$ as a function of the capacitance C_{cb}. The optimum capacitance C_{op} is the capacitance which makes maximum the quantity $\Delta\mathbf{P}_5$. The maximum of $\Delta\mathbf{P}_5$ is reached at $C_{op} = 805\,\mu$F ($f_{op} = 5\,$kHz).

complex three-dimensional geometries. The results given by our approach can be used to improve the coil design, to set the electrical parameters of the EMF system in its optimum values and to compute the workpiece deformation in a loose coupling strategy. Finally, we have shown that the numerical results provided by this method exhibit a good correlation with the results provided by other authors.

Acknowledgment

The work described in this paper and the research leading to these results has received funding from the Spanish Ministry of Education and Science through the National R+D Plan 2004-2007, reference DPI2006-15677-C02-01, SICEM project. The author also wants to acknowledge to Roger Mendez and Oscar Fruitos for their collaboration in the realization of this paper.

References

El-Azab, A., Garnich, M., Kapoor, A., 2003. Modeling of the electromagnetic forming of sheet metals: state-of-the-art and future needs. Journal of Materials Processing Technology 142, 744–754.

Fenton, G.K., Daehn, G.S., 1998. Modelling of electromagnetically formed sheet metal. Journal of Materials Processing Technology 75, 6–16.

Haiping, Y.U., Chunfeng, L.I., 2009. Effects of current frequency on electromagnetic tube compression. Journal of Materials Processing Technology 209, 1053–1059.

Jablonski, J., Winkler, R., 1978. Analysis of the electromagnetic forming process. International Journal of Mechanical Sciences 20, 315–325.

Jackson, J.D., 1999. Classical Electrodynamics. John Wiley & Sons, Inc., 3rd edition.

Mamalis, A.G., Manolakos, D.E., Kladas, A.G., Koumoutsos, A.K., 2006. Electromagnetic forming tools and processing conditions: numerical simulation. Materials and Manufacturing Processes 21, 411–423.

Motoasca, T.E., 2003. Electrodynamics in Deformable Solids for Electromagnetic Forming. Ph.D. thesis. Delft University of Technology.

Otin, R., 2010. Regularized Maxwell equations and nodal finite elements for electromagnetic field computations. Electromagnetics 30, 190–204.

Otin, R., 2011. ERMES user guide. Technical Report. International Center for Numerical Methods in Engineering (CIMNE), ref.: IT-617.

Otin, R., Mendez, R., Fruitos, O., 2012. A frequency domain approach for computing the Lorentz force in electromagnetic metal forming. Submitted.

Zhang, H., Murata, M., Suzuki, H., 1995. Effects of various working conditions on tube bulging by electromagnetic forming. Journal of Materials Processing Technology 48, 113–121.